

Nystrom method for the Muller boundary integral equations on a dielectric body of revolution: axially symmetric problem

Vitaliy S. Bulygin¹ ✉, Yuriy V. Gandel², Ana Vukovic³, Trevor M. Benson³, Phillip Sewell³, Alexander I. Nosich¹

¹Laboratory of Micro and Nano Optics, Institute of Radio-Physics and Electronics NASU, Kharkiv 61085, Ukraine

²Department of Mathematical Physics and Computational Mathematics, Kharkiv National University, Kharkov 61077, Ukraine

³George Green Institute for Electromagnetics Research, The University of Nottingham, Nottingham NG7 2RD, UK

✉ E-mail: vitaliy_bulygin@yahoo.com

ISSN 1751-8725

Received on 20th December 2014

Revised on 25th February 2015

Accepted on 27th February 2015

doi: 10.1049/iet-map.2014.0859

www.ietdl.org

Abstract: The authors consider the electromagnetic field in the presence of a dielectric body of revolution (BOR) in the axially symmetric case. The associated Muller boundary integral equation (IE) is reduced to a set of two IEs, further discretised using the Nystrom method. They derive a determinantal equation for the search of natural modes and present a new approach for the calculation of its roots. Results obtained are compared with known data for a dielectric sphere and a BOR generated by a super-ellipse as an approximation of a finite circular cylinder. The resonant frequencies and the Q-factors of the natural modes of a dielectric spheroid are studied.

1 Introduction

Dielectric resonators (DRs) are important elements of microwave and millimetre-wave integrated circuits used as filters, solid-state oscillator stabilisation cavities and antennas [1–7]. DRs are usually attractive because of their small size, mechanical simplicity and very small conduction losses. They can have relatively large or very narrow bandwidths, depending on the DR shape and working mode type. The knowledge of the resonance characteristics of isolated dielectric bodies is also of great interest for the optimal design of moderate-size dielectric lens antennas [8, 9].

The electromagnetic simulation of the natural modes of a DR, especially finding their Q-factors, requires high accuracy. For example, suppose that we are able to estimate complex modal frequency with a relative accuracy of 1%. If the imaginary part of the frequency, f_{im} , is 100 times smaller than real part, f_{re} , then the relative error of the f_{im} can be larger than 100%. This leads to incorrect calculation of Q-factors and modal field patterns. Today, complicated-shape DRs cannot be investigated accurately and quickly enough using the existing numerical simulation tools. Therefore several studies that considered DRs with a variety of shapes appeared – see [10–15].

An important sub-set of the great variety of DR shapes is body of revolution (BOR) configurations, such as the finite circular cylinder or sphere. The scattering of waves by a dielectric BOR was studied in [11–13] using a boundary integral equation (IE) method. The authors approximated the rotation contour C by a sequence of linear segments and used piece-wise constant or linear approximations to the Fourier components of electric and magnetic currents.

The alternative to widely used low-order projection methods is the recently developed locally corrected Nystrom method (LCNM). This method has been already used to solve boundary IEs in two-dimensional (2D) and 3D acoustic and electromagnetic scattering [16, 17]. The ‘local corrections’ mean that the length of the subinterval L containing a singular point is split into two parts. The first part, of length Δ , contains the kernel singular point, and the integral along this part is calculated using an adaptive quadrature or the Duffy transform. The other part has length $L-\Delta$ and the integral along this part can be handled with a standard quadrature. For better accuracy, the first part (i.e. Δ) has to be chosen as small as possible. However, if Δ is too small then the quadrature for the second part gives a poor approximation because

of the large value of the integrand derivative near the singularity. Thus, the LCNM needs a search for the optimal value of the parameter Δ ; this complicates the algorithm.

In this paper, we build a numerical solution of the Muller IE [18–20] for a BOR-DR in the axially symmetric case, using the entire-domain Nystrom method (NM) [20–24]. The central idea of the NM is the use of interpolation-type quadrature formulas to approximate the integrals. We interpolate the rotation contour and the unknown function with polynomials of degree n and take account of the IE kernels’ singular nature. A similar approach to the scattering associated with the Helmholtz equation was demonstrated in the recently published paper [25]. In contrast to conventional MoM, with segmentation of the contour and low-order local basis functions [10–15], our discretisation order is equal to n , which, to provide several-digit accuracy should be only slightly larger than the electrical size of the body. Thus, the NM is an economic mesh-less method that does not require numerical integrations. In the case of a smooth rotation contour, the NM gives extremely rapid convergence that enables high accuracy to be reached within reasonable computation time [22–24]. This is required in eigenvalue problems where one looks for the complex roots of the matrix determinant after the IE discretisation. For example, determinant calculation using the Gauss method requires $O(n^3)$, and therefore if we decrease discretisation order by a factor of 3 we decrease the calculation time by a factor of 27. In addition, the properties of our discretisation matrix allow us obtaining a solution with high accuracy (up to 10^{-7}); this is required in the analysis of high-Q whispering-gallery-like modes of dielectric open resonators [26] and sufficient for all results presented in the present paper.

The remainder of this paper is as follows. The boundary IEs for the axially symmetric excitation of a dielectric BOR are derived in Section 2. In Section 3, we discretise the obtained IEs using the NM. Section 4 is devoted to the determinant calculation. The results of the numerical experiments are presented in Section 5 and summarised in Section 6. The time dependence is selected as $\exp(-i\omega t)$ and omitted.

2 Integral equation

The total field $(\mathbf{E}_m, \mathbf{H}_m)$ inside and outside of a dielectric BOR is represented as a sum of the incident and scattered fields, that is,

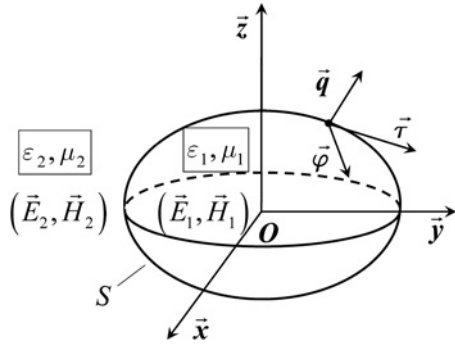


Fig. 1 Dielectric BOR and associated notations

$(\mathbf{E}_m, \mathbf{H}_m) = (\mathbf{E}_m^{\text{inc}}, \mathbf{H}_m^{\text{inc}}) + (\mathbf{E}_m^s, \mathbf{H}_m^s)$, where the region number is denoted by the subscript $m=1, 2$ (Fig. 1).

Magnetic and electric currents, $\mathbf{j}^m = \mathbf{E} \times \mathbf{n}$, $\mathbf{j}^e = \mathbf{n} \times \mathbf{H}$, satisfy the Muller IE (two coupled vector IEs) [17, 18] (see (1))

where (∇, f) divergence of f , $G_{1,2} = \exp(ik_{1,2}R)/(4\pi R)$ are the 3D scalar Green's functions, \mathbf{n} is the outer unit normal vector to the surface S , $k_{1,2}$ are the wavenumbers inside and outside S , respectively.

Note that the Muller IE is a Fredholm second-kind equation with square-integrable kernels [18]. Choose cylindrical coordinates ρ, φ, z and assume that the surface S is created by the rotation of contour C around the z -axis. Introduce also the curvilinear orthogonal coordinates q, τ and φ in terms of which S has the parameterisation

$$S: q = q_0, \quad \tau \in [-1, 1], \quad \varphi \in [0, 2\pi] \quad (2)$$

linked to the conventional cylindrical coordinates as

$$\rho = \rho(q, \tau), \quad z = z(q, \tau) \quad (3)$$

Here, the Lamé coefficients of the coordinates q, τ and φ are

$$l_q = \sqrt{(\rho'_q)^2 + (z'_q)^2}, \quad l_\tau = \sqrt{(\rho'_\tau)^2 + (z'_\tau)^2}, \quad l_\varphi = \rho \quad (4)$$

where prime means derivative with respect to subscript, and the unit vectors of curvilinear coordinates are

$$\mathbf{q} = (\mathbf{x} \cdot \rho'_q \cos \varphi + \mathbf{y} \cdot \rho'_q \sin \varphi + \mathbf{z} \cdot z'_q)/l_q \quad (5)$$

$$\boldsymbol{\tau} = (\mathbf{x} \cdot \rho'_\tau \cos \varphi + \mathbf{y} \cdot \rho'_\tau \sin \varphi + \mathbf{z} \cdot z'_\tau)/l_\tau \quad (6)$$

$$\boldsymbol{\varphi} = -\mathbf{x} \sin \varphi + \mathbf{y} \cos \varphi \quad (7)$$

Note that \mathbf{q} is the outer unit normal vector to the surface $S(\mathbf{q} = \mathbf{n})$ and $\boldsymbol{\tau}, \boldsymbol{\varphi}$ are tangential vectors to the same surface.

Furthermore, we will omit the function arguments for presentational clarity. In the case of the function argument being an integration variable, we will put sub-index '0', for example, ρ

$(q_0, t) = \rho_0$. Introduce the vector operators as

$$\mathbf{A}\mathbf{j} = \frac{i}{\omega} \iint_S \nabla \cdot (\nabla, (G_2 - G_1) \cdot \mathbf{j}) \, dS \quad (8)$$

$$\mathbf{B}\mathbf{j} = \frac{i}{\omega} \iint_S (k_2^2 G_2 - k_1^2 G_1) \cdot \mathbf{j} \, dS \quad (9)$$

$$\mathbf{C}(v)\mathbf{j} = \nabla \times \iint_S ((v_2 G_2 - v_1 G_1) \cdot \mathbf{j}) \, dS, \quad v = \varepsilon, \mu \quad (10)$$

$$\mathbf{f}_\varepsilon^E(P_0) = \varepsilon_2 \mathbf{E}_2^{\text{inc}}(P_0) + \varepsilon_1 \cdot \mathbf{E}_1^{\text{inc}}(P_0) \quad (11)$$

$$\mathbf{f}_\mu^H(P_0) = \mu_2 \cdot \mathbf{H}_2^{\text{inc}}(P_0) + \mu_1 \cdot \mathbf{H}_1^{\text{inc}}(P_0) \quad (12)$$

Using notations (8)–(12) and taking into account (5)–(7), rewrite the Muller IE (1) in the following form

$$(\boldsymbol{\tau}, -\mathbf{f}_\mu^H + \mathbf{A}\mathbf{j}^m + \mathbf{B}\mathbf{j}^m - \mathbf{C}(\mu)\mathbf{j}^e) = -j_\varphi^e \frac{\mu_2 + \mu_1}{2}, \quad (13)$$

$$(\boldsymbol{\varphi}, -\mathbf{f}_\varepsilon^E + \mathbf{A}\mathbf{j}^e + \mathbf{B}\mathbf{j}^e + \mathbf{C}(\varepsilon)\mathbf{j}^m) = -j_\tau^m \frac{\varepsilon_2 + \varepsilon_1}{2}$$

$$(\boldsymbol{\tau}, -\mathbf{f}_\varepsilon^E + \mathbf{A}\mathbf{j}^e + \mathbf{B}\mathbf{j}^e + \mathbf{C}(\varepsilon)\mathbf{j}^m) = j_\varphi^m \frac{\varepsilon_2 + \varepsilon_1}{2}, \quad (14)$$

$$(\boldsymbol{\varphi}, -\mathbf{f}_\mu^H + \mathbf{A}\mathbf{j}^m + \mathbf{B}\mathbf{j}^m - \mathbf{C}(\mu)\mathbf{j}^e) = j_\tau^e \frac{\mu_2 + \mu_1}{2}$$

where (\cdot, \cdot) means scalar product.

Now, consider the axially symmetric case where $\partial/\partial\varphi = 0$

$$\mathbf{j}_{\tau, \varphi}(t, \varphi) = \mathbf{j}_{s, \varphi}(t) \quad (15)$$

$$(\boldsymbol{\tau}, \mathbf{A}\mathbf{j}) = -\frac{i}{\omega} \frac{1}{l_\tau} \int_{-1}^1 \rho_0 \frac{\partial^2}{\partial \tau \partial t} (S_0^{(2)} - S_0^{(1)}) j_\tau \, dt \quad (16)$$

$$(\boldsymbol{\varphi}, \mathbf{A}\mathbf{j}) = 0 \quad (17)$$

$$(\boldsymbol{\tau}, \mathbf{B}\mathbf{j}) = \frac{i}{\omega l_\tau} \int_{-1}^1 \rho_0 \left\{ \rho'_\tau \rho'_\tau (k_2^2 S_1^{(2)} - k_1^2 S_1^{(1)}) + [z'_\tau z'_\tau (k_2^2 S_0^{(2)} - k_1^2 S_0^{(1)})] \right\} j_\tau \, dt \quad (18)$$

$$(\boldsymbol{\varphi}, \mathbf{B}\mathbf{j}) = \frac{i}{\omega} \int_{-1}^1 \rho_0 l_{0\tau} [k_2^2 S_1^{(2)} - k_1^2 S_1^{(1)}] j_\varphi \, dt \quad (19)$$

$$(\boldsymbol{\tau}, \mathbf{C}(v)\mathbf{j}) = \int_{-1}^1 \rho_0 h_\tau \frac{1}{l_q} \left(\frac{\partial}{\partial q} + \frac{\rho'_q}{l_q} \right) [v_2 S_1^{(2)} - v_1 S_1^{(1)}] j_\varphi \, dt \quad (20)$$

$$(\boldsymbol{\varphi}, \mathbf{C}(v)\mathbf{j}) = -\int_{-1}^1 \frac{\rho_0 l_{0\tau}}{l_{0q}} \left(\frac{\partial}{\partial q_0} + \frac{\rho'_{0q}}{l_{0q}} \right) [v_2 S_1^{(2)} - v_1 S_1^{(1)}] j_\tau \, dt \quad (21)$$

where $v = \varepsilon, \mu$ and the modal Green's function that is the M th component of the azimuthal Fourier series for the scalar Green function $\exp(-ikR)/R$, is defined as [22, 23]

$$S_M^{(m)} = \frac{1}{4\pi} \int_0^{2\pi} \frac{\exp(-ik_m L)}{L} \cos(M\psi) \, d\psi \quad (22)$$

$$\begin{aligned} \begin{pmatrix} -j_\tau^m \frac{\varepsilon_2 + \varepsilon_1}{2} \\ j_\tau^e \frac{\mu_2 + \mu_1}{2} \end{pmatrix} &= \mathbf{n} \times \begin{pmatrix} \varepsilon_2 \mathbf{E}_2^{\text{inc}} + \varepsilon_1 \mathbf{E}_1^{\text{inc}} \\ \mu_2 \mathbf{H}_2^{\text{inc}} + \mu_1 \mathbf{H}_1^{\text{inc}} \end{pmatrix} - \mathbf{n} \times \begin{pmatrix} \frac{i}{\omega} \iint_S [\nabla \cdot (\nabla, (G_2 - G_1) \cdot \mathbf{j}^e) + (k_2^2 G_2 - k_1^2 G_1) \cdot \mathbf{j}^e] \, dS \\ \frac{i}{\omega} \iint_S [\nabla \cdot (\nabla, (G_2 - G_1) \cdot \mathbf{j}^m) + (k_2^2 G_2 - k_1^2 G_1) \cdot \mathbf{j}^m] \, dS \end{pmatrix} \\ &+ \mathbf{n} \times \begin{pmatrix} \int \int_S \nabla \times [(\varepsilon_2 G_2 - \varepsilon_1 G_1) \cdot \mathbf{j}^m] \, dS \\ -\int \int_S \nabla \times [(\mu_2 G_2 - \mu_1 G_1) \cdot \mathbf{j}^e] \, dS \end{pmatrix} \end{aligned} \quad (1)$$

where $m = 1, 2$ and $L = [\rho^2 + \rho_0^2 - 2\rho\rho_0 \cos \psi + (z - z_0)^2]^{1/2}$. Note that we need only scalar Green function with index $M=0, 1$.

From (16) to (21) we can see that, in the axially symmetric case, (13) and (14) are independent IE sets with pairs of unknown functions, (j_φ^e, j_τ^e) for (13) and (j_φ^m, j_τ^e) for (14).

To simplify the notation we denote the integrand kernel of $(\xi, \Omega f)$, where $\xi = \tau$ or φ , and $\Omega = A, B, C(\varepsilon), C(\mu)$ as Ω_ξ . For example, in this notation

$$(\tau, A j^e) = \int_{-1}^1 A_\tau(\tau, t) j_\tau^e(t) dt,$$

$$A_\tau(\tau, t) = -\frac{i}{\omega} \frac{1}{l_\tau} \rho_0 \frac{\partial^2}{\partial \tau \partial t} [S_0^{(2)} - S_0^{(1)}]$$

Using asymptotic expressions of the first- and the second-kind elliptic integrals [27, 28], one can establish that

$$S_M^{(1,2)} \Big|_{t \rightarrow \tau} = -\frac{1}{2\pi\rho} \ln |\tau - t| + O(1) \quad (23)$$

$$\frac{\partial}{\partial q_0} S_M^{(1,2)} \Big|_{t \rightarrow \tau} = \frac{\rho'_q}{4\pi\rho^2} \ln |\tau - t| + O(1) \quad (24)$$

$$\frac{\partial^2}{\partial \tau \partial t} [S_M^{(2)} - S_M^{(1)}] \Big|_{t \rightarrow \tau} = \frac{-k_2^2 + k_1^2}{4\pi\rho} (\rho^2 + z^2) \ln |\tau - t| + O(1) \quad (25)$$

The parts $O(1)$ in (23)–(25) belong to the space $C^{1,\alpha}[-1, 1]$ for $0 < \alpha < 1$. The space $C^{p,\alpha}[a, b]$ consists of the functions whose p th derivatives satisfy the Hölder condition with coefficient α on $[a, b]$.

Therefore all singularities in the IEs (13) and (14) are indeed integrable as expected for the Fredholm second-kind IEs. Using (23)–(25) we can separate logarithmic singularities explicitly; this is beneficial for correct use of interpolation-type quadratures in the discrete model of Muller IE. In the axially symmetric case the IE set (14) reduces to

$$\frac{-1}{2} \begin{pmatrix} j_\varphi^m(\varepsilon_2 + \varepsilon_1) \\ j_\tau^e(\mu_2 + \mu_1) \end{pmatrix} + \int_{-1}^1 \begin{pmatrix} K_{\tau\tau}(\tau, t) & K_{\tau\varphi}(\tau, t) \\ K_{\varphi\tau}(\tau, t) & K_{\varphi\varphi}(\tau, t) \end{pmatrix} \begin{pmatrix} j_\tau^e(t) \\ j_\varphi^m(t) \end{pmatrix} dt$$

$$+ \begin{pmatrix} c_{\tau\tau}(\tau) & c_{\tau\varphi}(\tau) \\ c_{\varphi\tau}(\tau) & c_{\varphi\varphi}(\tau) \end{pmatrix} \cdot \int_{-1}^1 \begin{pmatrix} j_\tau^e(t) \\ j_\varphi^m(t) \end{pmatrix} \ln |\tau - t| dt = \begin{pmatrix} (\tau, f_\mu^H) \\ (\varphi, f_\mu^H) \end{pmatrix} \quad (26)$$

where

$$c_{\tau\tau}(\tau) = \frac{-1}{4\pi} \frac{i}{\omega l_\tau} (k_1^2 - k_2^2) (\rho^2 + z^2) \quad (27)$$

$$c_{\tau\varphi}(\tau) = \frac{-1}{4\pi} \frac{\rho'_q \cdot l_\tau}{\rho \cdot l_q} (\varepsilon_2 - \varepsilon_1) \quad (28)$$

$$c_{\varphi\tau}(\tau) = \frac{1}{4\pi} \frac{\rho'_q \cdot l_\tau}{\rho \cdot l_q} (\mu_2 - \mu_1) \quad (29)$$

$$c_{\varphi\varphi}(\tau) = -\frac{i}{2\pi} \frac{l_\tau}{\omega} (k_2^2 - k_1^2) \quad (30)$$

$$K_{\tau\tau}(\tau, t) = A_\tau(\tau, t) + B_\tau(\tau, t) - c_{\tau\tau}(\tau) \ln |\tau - t| \quad (31)$$

$$K_{\tau\varphi}(\tau, t) = C_\tau^e(\tau, t) - c_{\tau\varphi}(\tau) \ln |\tau - t| \quad (32)$$

$$K_{\varphi\tau}(\tau, t) = -C_\tau^m(\tau, t) - c_{\varphi\tau}(\tau) \ln |\tau - t| \quad (33)$$

$$K_{\varphi\varphi}(\tau, t) = A_\varphi(\tau, t) + B_\varphi(\tau, t) - c_{\varphi\varphi}(\tau) \ln |\tau - t| \quad (34)$$

To obtain the equivalent of (13) in the axially symmetric case, one

has to exchange, in (26)–(34), ε_i with μ_i and E_i^0 with H_i^0 ($i = 1, 2$), then in the first equation of (13) replace j_φ^m with $-j_\varphi^e$ and j_τ^e with j_τ^m , and similarly in the second equation of (13) replace j_φ^m with j_φ^e and j_τ^e with $-j_\tau^m$. Note that the kernels $K_{\xi\xi}(\tau, t)$, where $\xi = \tau, \varphi, \zeta = \tau, \varphi$ belong to the space $C^{p,\alpha}[-1, 1]$ for any $0 < \alpha < 1$, where $p = \min\{1, s\}$, and s is the smoothness order of the rotation contour.

3 Discretisation of IEs

Before discretising the IEs derived, we note that there are no contour or field singularities at the poles of S . Therefore we can approximate the unknown components of electric and magnetic currents with the interpolation polynomials and use the following quadrature formulas [27, 28]

$$\int_{-1}^1 u_{n-1}(t) dt = \sum_{p=0}^{n-1} A_p^n u_{n-1}(x_p) \quad (35)$$

$$\int_{-1}^1 u_{n-1}(t) \ln |\tau - t| dt = \sum_{p=0}^{n-1} u_{n-1}(x_p) L_p(\tau) \quad (36)$$

$$L_p(\tau) = A_p^n \left\{ \frac{1}{2} \ln(1 - \tau^2) + Q_1(\tau) + \sum_{m=1}^{n-1} P_m(x_p) [Q_{m+1}(\tau) - Q_{m-1}(\tau)] \right\} \quad (37)$$

where $A_p^n = 2(1 - x_p^2)^{-1} P_n'(x_p)^{-2}$, $u_{n-1}(t)$ is a polynomial of degree $n - 1$, $P_m(x)$ is the Legendre polynomial of the degree m , x_p is the p th root of the Legendre polynomial of the degree n and $Q_m(\tau)$ is the Legendre function of the first kind.

Using (35)–(37), we obtain a discrete counterpart of IE (26), that is, a matrix equation in the form

$$Ay = b \quad (38)$$

where

$$A = \begin{pmatrix} C^{\tau\tau} & C^{\tau\varphi} \\ C^{\varphi\tau} & C^{\varphi\varphi} \end{pmatrix} \quad (39)$$

$$C_{mp}^{1\tau} = c_{\tau\tau}(x_m) L_p(x_m) + A_p^n K_{\tau\tau}(x_m, x_p) \quad (40)$$

$$C_{mp}^{\tau\varphi} = \delta_{mp} + c_{\tau\varphi}(\tau) L_p(x_m) + A_p^n K_{\tau\varphi}(x_m, x_p) \quad (41)$$

$$C_{mp}^{\varphi\tau} = -\delta_{mp} + A_p^n K_{\varphi\tau}(x_m, x_p) \quad (42)$$

$$C_{mp}^{\varphi\varphi} = c_{\varphi\varphi}(x_m) L_p(x_m) + A_p^n K_{\varphi\varphi}(x_m, x_p) \quad (43)$$

$$b = (b^\tau \quad b^\varphi)^\top, \quad y = (y^\tau \quad y^\varphi)^\top \quad (44)$$

$$b_m^\tau = (\tau, f_\mu^H)(x_m) \quad (45)$$

$$b_m^\varphi = (\varphi, f_\mu^H)(x_m) \quad (46)$$

and $m, p = 0, 1, \dots, n-1$.

The solutions are polynomials $j_\tau^{e(n-1)}(t)$ and $j_\varphi^{m(n-1)}(t)$: $j_\tau^{e(n-1)}(x_m) = y_m^\tau$ and $j_\varphi^{m(n-1)}(x_m) = y_m^\varphi$.

Convergence rate of the presented numerical scheme depends on the smoothness of the kernels $K_{\xi\xi}(\tau, t)$, $\xi = \tau, \varphi$ and $\zeta = \tau, \varphi$. Assume that $K_{\xi\xi}(\tau, t) \in C^{p,\alpha}[-1, 1]$ and functions $j_\tau^e(t), j_\varphi^m(t)$ are the exact

solutions of the IE (26). Then

$$\|j_v^{e(n-1)}(t) - j_v^e(t)\|_2 < \frac{c}{n^{p+\alpha}}, \quad v = \tau, \varphi$$

where $\|\cdot\|_2$ is the $L_2[-1, 1]$ norm. This means that if the rotation contour smoothness order is not smaller than 1, then in our case the rate of convergence is $c/n^{2-\alpha}$, where ‘2-0’ means a number arbitrarily close to but smaller than the number ‘2’.

4 Determinant root approximation

Accurate calculation of the complex roots of determinantal equations has high numerical complexity because the imaginary part of practically useful roots is much smaller than the real part. Note that the determinant is holomorphic as a function of the wavenumber. From well-known theorems of complex analysis, it follows that if two holomorphic functions are equal on any finite real-valued interval, then they are the same. One can also prove that if two holomorphic functions are close to each other on some real-valued interval (a, b) , then they are close for all $z: \{\text{Re } z \in (a, b), |\text{Im } z| < \delta\}$. Denote the determinant of the matrix A in discrete counterpart (38) for complex wavenumber z as $\text{Det}(z)$. For $\delta = (b - a)/5$, we approximate $\text{Det}(z)$ by the interpolation polynomial of degree $m-1$ as follows

$$\text{Det}(z) \simeq \text{Det}_{m-1}(z) = \text{Det}_{m-1}^{\text{Re}}(z) + i \cdot \text{Det}_{m-1}^{\text{Im}}(z) \quad (47)$$

and approximate real and imaginary parts of the determinant with interpolation polynomials at the Chebyshev points

$$\text{Det}_{m-1}^{\text{Re, Im}}(x) \simeq \sum_{j=0}^{m-1} f_j^{\text{Re, Im}} l_{m-1,j}[y(x)] \quad (48)$$

where

$$l_{m-1,j}(x) = \frac{T_m(t)}{T_m(t_j^*)(t - t_j^*)} \quad (49)$$

is the fundamental interpolation polynomial of degree $m-1$, $f_j^{\text{Re, Im}} = \{\text{Re}, \text{Im}\} \text{Det}[\tau(t_j^*)]$, $\tau(t) = (a/2)(1-t) + (b/2)(1+t)$, $y(x) = (2x - a - b)/(b - a)$ and nominator of (49) is Chebyshev polynomial of the first kind. Approximation (48) has exponential convergence on (a, b) .

The method presented above gives remarkable advantage in the determinant root investigation, because the calculation of $\text{Det}_{m-1}(z)$ becomes extremely fast. For example, the choice of $m = 40$ gives us sufficient determinant approximation to obtain four complex frequencies of a dielectric sphere of $\epsilon = 38$ as shown in Fig. 2. This is supported by Fig. 3, where we show the relative difference between the exact values of determinant and those

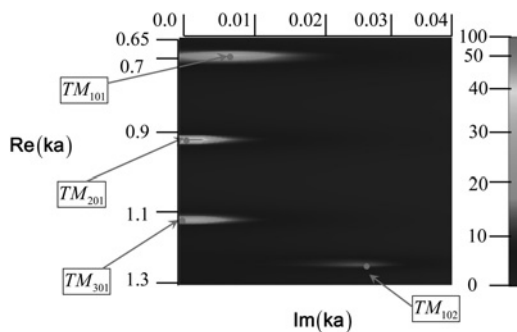


Fig. 2 Relief of $1/\text{Det}(z)$ for $\text{Re}(ka) \in (0.65, 1.3)$, $\text{Im}(ka) \in (0, 0.04)$ in the TM case of a dielectric sphere with $\epsilon = 38$, discretisation order $n = 16$

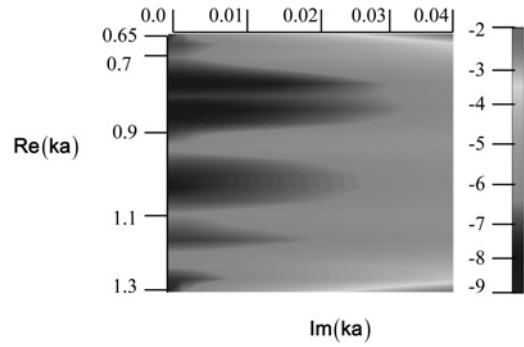


Fig. 3 Relative error of the determinant approximation (49) on a logarithmic scale for $\text{Re}(ka) \in (0.65, 1.3)$, $\text{Im}(ka) \in (0, 0.04)$, a is the sphere radius, interpolation degree $m = 40$, TM case of a dielectric sphere with $\epsilon = 38$ and discretisation order $n = 16$

obtained from (47), on the complex plane of ka , k being the wavenumber of the host medium.

5 Numerical experiments

5.1 Validation: dielectric sphere

The equations for the complex frequencies of the (transverse electric) TE_{vpr} and (transverse magnetic) TM_{vpr} modes of a dielectric sphere are [29, 30]

$$\text{TM: } \frac{J_{v-1/2}(m \cdot x)}{J_{v+1/2}(m \cdot x)} = m \frac{H_{v-1/2}^{(2)}(x)}{H_{v+1/2}^{(2)}(x)} - v \frac{m^2 - 1}{m} \quad (50)$$

$$\text{TE: } \frac{J_{v-1/2}(m \cdot x)}{J_{v+1/2}(m \cdot x)} = \frac{1}{m} \frac{H_{v-1/2}^{(2)}(x)}{H_{v+1/2}^{(2)}(x)} \quad (51)$$

where the indices v, p and r denote the number of the field variations in the elevation-angle, azimuthal and radial directions, respectively [3, 31], the sphere refractive index is $m = \sqrt{\epsilon}$, ϵ is the relative permittivity, $x = ka$ and a is the sphere radius.

In Table 1, we compare the complex wavenumbers of four lowest axially symmetric modes found from (50) and (51) with the same values found using the NM of the order $n = 256$. They show five coinciding digits.

In Fig. 4, we show the relative errors in ka as a function of discretisation order n , introduced as $(k - k_n)/k = c/n^\alpha$, where k and k_n are the exact and the approximate values, respectively. Then $\chi = \log[(k - k_n)/k] = \log c - \alpha \log n$ and χ is a linear function of $\log n$. Therefore α is the tangent of the angle between $\chi \log n$ and the abscissa. Using the data from Fig. 4, we can conclude that the rate of convergence in the case of dielectric sphere can be approximated as c/n^3 .

5.2 Validation: finite circular dielectric cylinder

As our method requires a smooth contour of the BOR cross-section, we approximate the contour of a finite circular cylinder (or pillbox)

Table 1 Normalised wavenumbers of the lowest axially symmetric modes of a dielectric sphere with $\epsilon = 38$

	Exact values of ka	ka values for $n = 256$
TE ₁₀₁	0.4988640135 + 0.0053824112 <i>i</i>	0.4988643588 + 0.0053826785 <i>i</i>
TE ₂₀₁	0.7217032171 + 0.0006767775 <i>i</i>	0.7217039554 + 0.0006768466 <i>i</i>
TM ₁₀₁	0.7039442495 + 0.0081520954 <i>i</i>	0.7039446891 + 0.0081518508 <i>i</i>
TM ₂₀₁	0.9205428124 + 0.0004519837 <i>i</i>	0.9205436438 + 0.0004520077 <i>i</i>

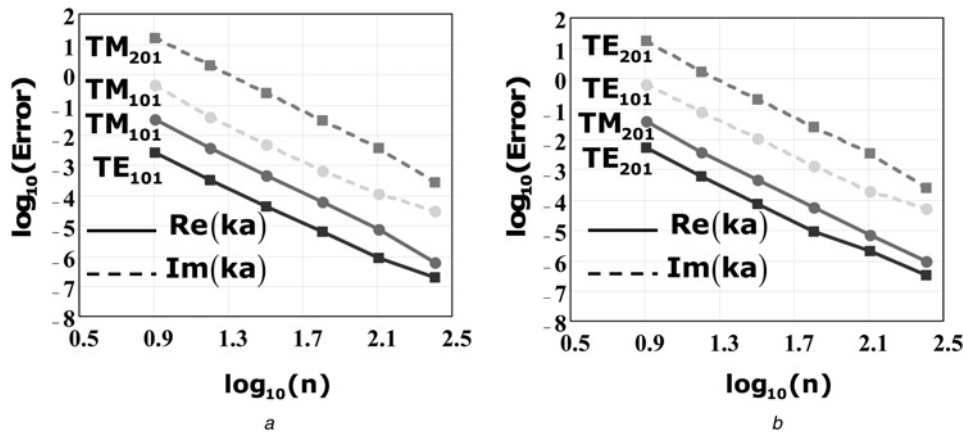


Fig. 4 Relative errors in the complex wavenumbers of the natural modes as a function of $\log n$, for $n = 8, 16, 32, 64, 128, 256$

a Imaginary part of TM₂₀₁, TM₁₀₁ and real part of TM₁₀₁, TE₁₀₁
b Imaginary part of TE₂₀₁, TE₁₀₁ and real part of TM₂₀₁, TE₂₀₁

with a half of super-ellipse (Fig. 5)

$$\rho(t) = a \cdot r(t) \cdot \sin t, \quad z(t) = b \cdot r(t) \cdot \cos t \quad (52)$$

$$r(t) = [\cos^{2N}(t) + \sin^{2N}(t)]^{-1/2N} \quad (53)$$

In [5], the approximate expressions for the real parts of the wavenumbers and the Q-factors of the TM_{01δ} and TE_{01δ} modes of a pillbox DR have been presented. Here, the index $\nu=0$ means the absence of field variation in azimuth, and the index $p=1$ denotes single variation along the radius. The last index δ indicates symbolically that the height h of the pillbox is smaller than $\lambda_g/2$, where λ_g is the wavelength of the TM₀₁ or TE₀₁ dielectric waveguide mode [3, 31].

The authors used the IE method described in [11, 12] to calculate complex modal wavenumbers for different ratios a/h ($h=2b$), and

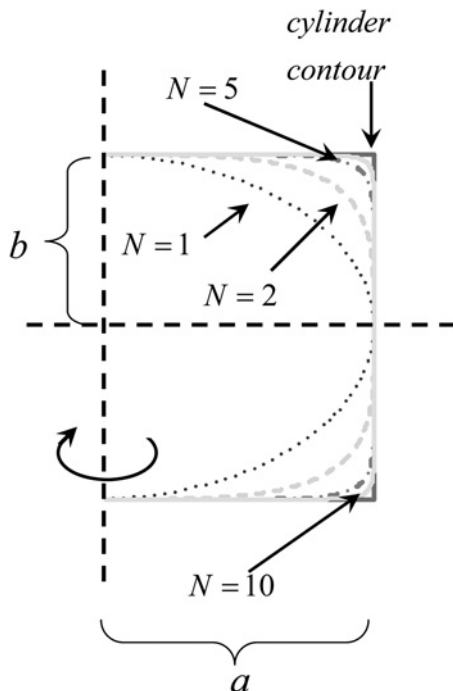


Fig. 5 BOR contour represented using a half of super-ellipse

further derived the curve-fit equations as

$$(ka)^{\text{TE}} = 2.920415 \cdot \varepsilon^{-0.465421} \times [0.690841 + 0.319075(a/h) - 0.035494(a/h)^2] \quad (54)$$

$$Q^{\text{TE}} = 0.012356 \cdot \varepsilon^{1.207086} \times [5.2696(a/h) + 106.18807(a/h)^{0.624875} e^{-1.027195(a/h)}] \quad (55)$$

$$(ka)^{\text{TE}} = 2.932566 \cdot \varepsilon^{-0.467715} \{1 - [0.075 - 0.05(a/h)] \times (1/28)(\varepsilon - 10)\} \times \{1.047542 + 0.377422(a/h) + 0.07112(a/h)^2\} \quad (56)$$

$$Q^{\text{TE}} = 0.008721 \cdot \varepsilon^{0.888413} e^{0.0397475 \cdot \varepsilon} \{1 - [0.3 - 0.2(a/h)](1/28) \cdot (38 - \varepsilon)\} [9.498196(a/h) + 2058.33(a/h)^{4.322261} e^{-3.50099(a/h)}] \quad (57)$$

In Figs. 6 and 7, we present a comparison between the data calculated from (55) to (57) and those obtained by our method, for the TM_{01δ} and TE_{01δ} modes of a pillbox DR with $\varepsilon = 38$.

They demonstrate remarkably good agreement that may serve as a validation of the NM algorithm proposed in this paper. Still as our method possesses a guaranteed convergence, and that of [11, 12] does not, the agreement, in fact, validates the results of [11, 12].

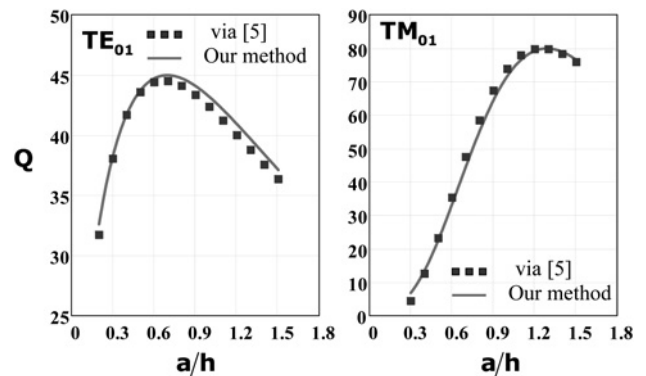


Fig. 6 Dielectric pillbox mode Q-factors as a function of a/h using the method of [5] and our method

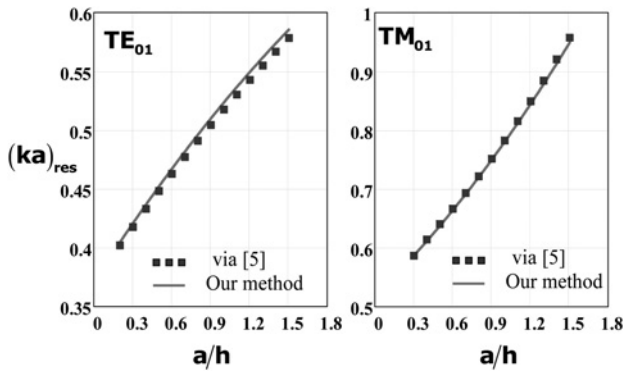


Fig. 7 Real part of a dielectric pillbox mode wavenumber as a function of a/h using the method of [5] and our method

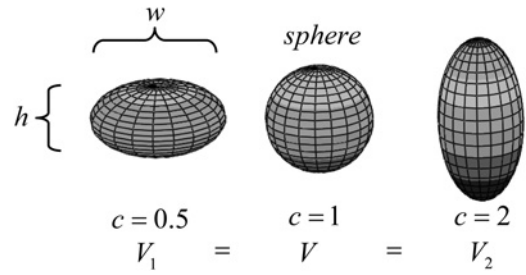


Fig. 8 Equal volume spheroids with different values of ratio c

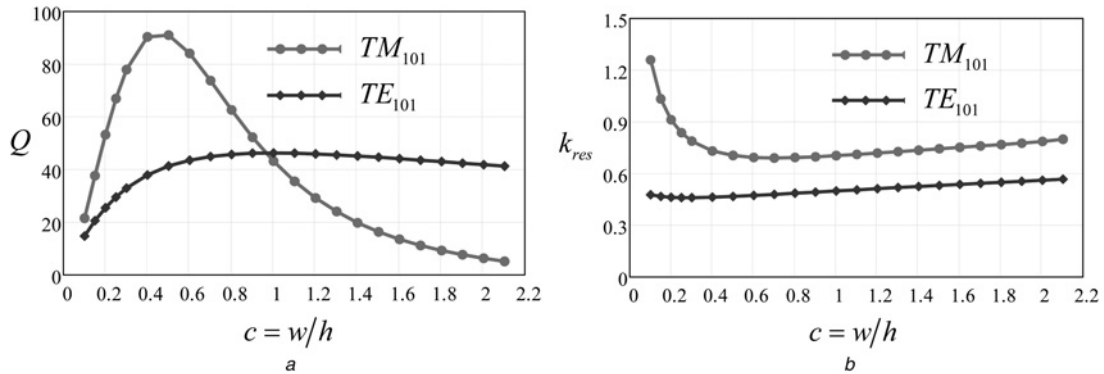


Fig. 9 Function of the spheroid deformation parameter c for the TM_{101} and TE_{101} modes, $\epsilon = 38$

a Q-factors
b Resonant frequencies

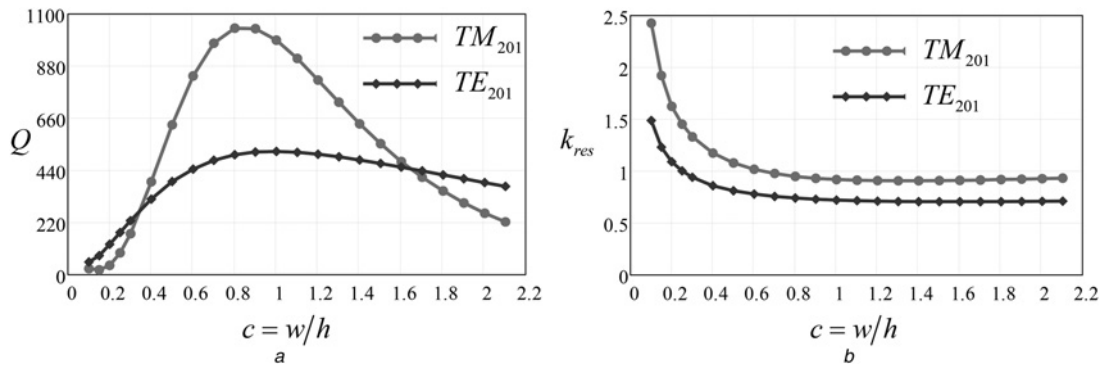


Fig. 10 Same as in Fig. 9 however for the TM_{201} and TE_{201} modes

5.3 Optimisation of a dielectric spheroid

In the theory of microwave DRs, an interesting question arises: Can one prolate or oblate a dielectric sphere so that the mode of the dielectric spheroid obtained would have a larger Q-factor than for a dielectric sphere of the same volume? To answer the question we have to calculate Q-factors of spheroids with different ratios $c = h/w$, where h and w are the spheroid height and diameter (Fig. 8).

Assume that the centre of the spheroid considered is at the origin. Then its contour has the following parameterisation

$$\rho(t) = c^{-1/3} \cdot \sin t, \quad z(t) = c^{2/3} \cdot \cos t \quad (58)$$

To find the complex modal wavenumbers for slightly prolate or oblate spheroids, we search for the minima of the determinant (49) for a sphere ($c=1$) as initial data. Then we change the ratio c , take the modal

wavenumber at the previous step as new initial data and continue iterations to convergence. The results are shown in Figs. 9 and 10.

As one can see from Fig. 9a if the DR volume is fixed, then for the TE_{101} mode the sphere gives the largest Q-factor. However, for the TM_{101} mode the oblate spheroid with parameter $c=0.5$ gives a Q-factor that is more than two times larger than that of the sphere.

From Fig. 9b, we can also conclude that for both the TE_{101} and TM_{101} modes, the real part of the modal wavenumber is, in general, close to its value for a dielectric sphere. A larger deviation from that value is observed for the TM_{101} mode only when c gets smaller than 0.3; this is accompanied by a sharp decline in the mode Q-factor.

For the TM_{201} mode, Fig. 10 shows us that a spheroid with $c=0.8$ has 6% higher Q-factor than the sphere. From our numerical experiments, it turns out that for higher-order axially symmetric modes the sphere has the largest Q-factor. Thus, the answer to the

question formulated above is positive but only for a few lowest axially symmetric TM modes of the spheroid.

6 Conclusions

We have presented a Nystrom-type numerical algorithm for the analysis of the wave-scattering and eigenvalue problems associated with dielectric BOR objects, in the axially symmetric case. The numerical results related to the natural modes whose fields have no variations along the azimuth have been demonstrated. They have enabled us to validate the method and the developed algorithm. Using this computational instrument, we have performed elementary optimisation of the shape of an arbitrary lossless dielectric spheroid DR aimed at the maximisation of the Q-factors of the four lowest axially symmetric modes. Here, the Q-factor of the TM_{101} mode can be made twice larger if the spheroid is oblate, with the height-to-width ratio being 0.5, whereas all other modes show the largest Q-factors if the DR is just a sphere.

7 References

- 1 Fiedziuszko, S.J., Holme, S.: 'Dielectric resonators raise your high-Q', *IEEE Microw. Mag.*, 2001, **2**, (3), pp. 50–60
- 2 Ishihara, O., Mori, T., Sawano, M., Nakatani, M.: 'A highly stabilized GaAs FET oscillator using a dielectric resonator feedback circuit in 9–14 GHz', *IEEE Trans. Microw. Theory Tech.*, 1980, **28**, (8), pp. 817–824
- 3 Mongia, R., Bharia, P.: 'Dielectric resonator antennas – a review and general design relations for resonant frequency and bandwidth', *Int. J. Microw. Millim.-Wave Comput.-Aided Eng.*, 1994, **4**, (3), pp. 230–247
- 4 Petosa, A., Ittipiboon, A., Antar, Y.M.M., Roscoe, D., Cuhaci, M.: 'Recent advances in dielectric-resonator antenna technology', *IEEE Antennas Propag. Mag.*, 1998, **49**, (3), pp. 35–48
- 5 Kishk, A.A., Glisson, A.W.: 'Bandwidth enhancement for split cylindrical dielectric resonator antennas', *Prog. Electromagn. Res.*, 2001, **33**, pp. 97–118
- 6 Vahala, K.J.: 'Optical microcavities', *Nature*, 2003, **424**, pp. 839–846
- 7 Simeoni, M., Cicchetti, R., Yarovoy, A., Caratelli, D.: 'Plastic-based supershaped dielectric resonator antennas for wide-band applications', *IEEE Trans. Antennas Propag.*, 2011, **59**, (12), pp. 4820–4825
- 8 Available at <http://www.antennacompany.com>
- 9 Boriskin, A.V., Sauleau, R., Nosich, A.I.: 'Exact off-resonance near fields of small-size extended hemielliptic lenses illuminated by plane waves', *J. Opt. Soc. Am. A*, 2009, **26**, (2), pp. 259–264
- 10 Llombart, N., Neto, A.: 'THz time-domain sensing: the antenna dispersion problem and a possible solution', *IEEE Trans. Terahertz Sci. Technol.*, 2012, **2**, (4), pp. 416–423
- 11 Glisson, A.W., Kajfez, D., James, J.: 'Evaluation of modes in dielectric resonators using a surface integral equation formulation', *IEEE Trans. Microw. Theory Tech.*, 1983, **31**, pp. 1023–1029
- 12 Kajfez, D., Glisson, A.W., James, J.: 'Computed modal field distribution for isolated dielectric resonators', *IEEE Trans. Microw. Theory Tech.*, 1984, **32**, (12), pp. 1609–1616
- 13 Magoulas, A.N., Fikioris, J.G.: 'Scattering from axisymmetric dielectric scatterers: a hybrid method of solving the surface integral equations', *IEEE Trans. AP*, 2007, **55**, pp. 2811–2823
- 14 Junker, G.P., Kishk, A.A., Glisson, A.W.: 'Input impedance of dielectric resonator antennas excited by a coaxial probe', *IEEE Trans. Antennas Propag.*, 1994, **42**, (7), pp. 960–966
- 15 Junker, G.P., Kishk, A.A., Glisson, A.W.: 'Input impedance of aperture coupled dielectric resonator antennas', *IEEE Trans. Antennas Propag.*, 1996, **44**, (5), pp. 600–607
- 16 Canino, L.F., Ottusch, J.J., Stalzer, M.A., Visher, J.L., Wandzura, S.M.: 'Numerical solution of the Helmholtz equation in 2D and 3D using a high-order Nyström discretization', *J. Comput. Phys.*, 1998, **146**, (2), pp. 627–663
- 17 Fleming, J.L., Wood, A.W., Wood, W.D. Jr.: 'Locally corrected Nystrom method for EM scattering by bodies of revolution', *J. Comput. Phys.*, 2004, **196**, pp. 41–52
- 18 Muller, C.: 'Foundations of the mathematical theory of electromagnetic wave' (Springer-Verlag, Berlin, 1969)
- 19 Harrington, R.F.: 'Boundary integral formulations for homogeneous material bodies', *J. Electromagn. Waves Appl.*, 1989, **3**, pp. 1–15
- 20 Burghignoli, P., Di Nallo, C., Frezza, F., Galli, A.: 'A simple Nystrom approach for the analysis of 3D arbitrarily shaped conducting and dielectric bodies', *Int. J. Numer. Model., Electron. Netw. Devices Fields*, 2003, **16**, (1), pp. 179–194
- 21 Balaban, M.V., Smotrova, E.L., Shapoval, O.V., Bulygin, V.S., Nosich, A.I.: 'Nystrom-type techniques for solving electromagnetics integral equations with smooth and singular kernels', *Int. J. Numer. Model., Electron. Netw. Devices Fields*, 2012, **25**, (5–6), pp. 490–511
- 22 Bulygin, V.S., Nosich, A.I., Gandel, Y.V.: 'Nystrom-type method in three-dimensional electromagnetic diffraction by a finite PEC rotationally symmetric surface', *IEEE Trans. Antennas Propag.*, 2012, **60**, (10), pp. 4710–4718
- 23 Bulygin, V.S., Benson, T.M., Gandel, Y.V., Nosich, A.I.: 'Full-wave analysis and optimization of a TARA-like shield-assisted paraboloidal reflector antenna using a Nystrom-type method', *IEEE Trans. Antennas Propag.*, 2013, **61**, (10), pp. 4981–4989
- 24 Tsalamengas, J.L.: 'Exponentially converging Nystrom method in oblique diffraction of arbitrarily polarized waves by bianisotropic/chiral cylinders with arbitrary smooth cross section', *IEEE Trans. Antennas Propag.*, 2013, **61**, (7), pp. 3362–3673
- 25 Helsing, J., Karlsson, A.: 'An explicit kernel-split panel-based Nystrom scheme for integral equations on axially symmetric surfaces', *J. Comput. Phys.*, 2014, **272**, pp. 686–703
- 26 Ryu, H.-Y., Notomi, M., Kim, G.-H., Lee, Y.-H.: 'High quality-factor whispering-gallery mode in the photonic crystal hexagonal disk cavity', *Opt. Express*, 2004, **12**, (8), pp. 1709–1718
- 27 Gradshteyn, I.S., Ryzhik, I.M.: 'Table of integrals, series, and products' (Academic Press, Inc., Moscow, 1994)
- 28 Abramowitz, M., Stegun, I.A.: 'Handbook of mathematical functions' (National Bureau of Standards Publ., Applied Mathematics Series, Dover Publications, Mineola, 1964)
- 29 Gastine, M., Courtois, L., Dormann, J.L.: 'Electromagnetic resonances of free dielectric spheres', *IEEE Trans. Microw. Theory Tech.*, 1967, **15**, pp. 694–700
- 30 Affolter, P., Eliasson, E.: 'Electromagnetic resonances and Q-factors of lossy dielectric spheres', *IEEE Trans. Microw. Theory Tech.*, 1973, **21**, (9), pp. 573–578
- 31 Pozar, D.: 'Microwave engineering' (Wiley, Hoboken, NJ, USA, 2011, 4th edn.)